JOURNAL OF GEOPHYSICAL RESEARCH, VOL. 98, NO. D6, PAGES 10,751–10,762, JUNE 20, 1993

The Upper Atmosphere Research Satellite Microwave Limb Sounder Instrument

F. T. BARATH,[1] M. C. CHAVEZ,[1] R. E. COFIELD,[1] D. A. FLOWER,[1] M. A. FRERKING,[1] M. B. GRAM,[1] W. M. HARRIS,[1] J. R. HOLDEN,[1] R. F. JARNOT,[1] W. G. KLOEZEMAN,[1] G. J. KLOSE,[1] G. K. LAU,[1] M. S. LOO,[1] B. J. MADDISON,[2] R. J. MATTAUCH,[3] R. P. MCKINNEY,[1] G. E. PECKHAM,[4] H. M. PICKETT,[1] G. SIEBES,[1] F. S. SOLTIS,[1] R. A. SUTTIE,[4] J. A. TARSALA,[1] J. W. WATERS,[1] AND W. J. WILSON[1]

The microwave limb sounder (MLS) on the Upper Atmosphere Research Satellite (UARS) is the first satellite experiment using limb sounding techniques at microwave frequencies. Primary measurement objectives are stratospheric ClO, O_3, H_2O, temperature, and pressure. Measurements are of thermal emission: all are performed simultaneously and continuously and are not degraded by ice clouds or volcanic aerosols. The instrument has a 1.6-m mechanically scanning antenna system and contains heterodyne radiometers in spectral bands centered near 63, 183, and 205 GHz. The radiometers operate at ambient temperature and use Schottky-diode mixers with local oscillators derived from phase-locked Gunn oscillators. Frequency tripling by varactor multipliers generates the 183- and 205-GHz local oscillators, and quasi-optical techniques inject these into the mixers. Six 15-channel filter banks spectrally resolve stratospheric thermal emission lines and produce an output spectrum every 2 s. Thermal stability is sufficient for "total power" measurements which do not require fast chopping. Radiometric calibration, consisting of measurements of cold space and an internal target, is performed every 65-s limb scan. Instrument in-orbit performance has been excellent, and all objectives are being met.

INTRODUCTION

The Upper Atmosphere Research Satellite (UARS) launched by the Space Shuttle Discovery on September 12, 1991, is a NASA mission dedicated to the comprehensive and integrated study of the Earth's upper atmosphere [*Reber*, 1990]. The microwave limb sounder (MLS), one of 10 UARS instruments, was developed by the Jet Propulsion Laboratory in the United States with the 183-GHz radiometer subsystem provided by Heriot-Watt University and Rutherford Appleton Laboratory in the United Kingdom. Prior development included aircraft [*Waters et al.*, 1979, 1980] and balloon [*Waters et al.*, 1981, 1984, 1988; *Robbins et al.*, 1990] experiments.

The primary measurement objectives of UARS MLS, shown in Figure 1, are ClO (~15–45 km in altitude), O_3 (~15–80 km), H_2O (~15–85 km), temperature (~30–60 km), and pressure (~30–60 km). ClO is the rate limiting molecule in chlorine destruction of O_3, and its abundance is a measure of the rate at which chlorine destroys ozone. ClO measurement on a global scale by MLS is important for understanding and monitoring chlorine depletion of ozone. Simultaneous MLS measurements of O_3 and H_2O provide additional information on stratospheric ozone chemistry. The H_2O and O_3 measurements are to higher altitudes than previously explored on a global basis and will provide new information on chemistry in the mesosphere. Pressure measurements from O_2 lines provide the vertical reference for composition measurements. Secondary MLS measurement goals include H_2O_2, HNO_3, volcanic injections of SO_2, and one component of wind in the mesosphere. All measurements are performed continuously, day and night. An important feature of the MLS is that its measurements are not degraded by ice clouds (such as the polar stratospheric clouds on which heterogeneous chemistry detrimental to ozone can occur) or volcanic aerosols (such as those from the Pinatubo volcano which erupted a few months before the UARS launch).

The MLS field of view (FOV) is directed 90° from the UARS orbital velocity, and the tangent point of the observation path (where the signals mostly originate) is approximately 23° great circle distance from the suborbital track of the satellite. The 57° inclination of the UARS orbit thus allows MLS to perform measurements from 34° latitude on one side of the equator to 80° on the other. UARS performs a 180° "yaw maneuver" 10 times per year, allowing MLS and other instruments to alternately view northern and southern high latitudes with a periodicity of about 36 days (this varies a few days through a yearly cycle). Local solar times at measurement locations do not vary appreciably with longitude on a given day but can vary greatly with latitude. The UARS orbit plane precesses so that all local times are covered at all latitudes during each ~36-day period.

This paper describes the UARS MLS instrument, and the reader is referred to *Waters* [1989, 1992] for a discussion of the measurement technique. Future publications will give details of instrument calibration, data processing algorithms, the validation of data, and scientific results.

INSTRUMENT OVERVIEW

Table 1 lists MLS measurement bands, and a simplified instrument block diagram is shown in Figure 2. An antenna receives radiation from the atmospheric limb and is mechanically scanned in the vertical. The switching mirror accepts radiation either from the antenna or, for calibration, from an

[1]Jet Propulsion Laboratory, California Institute of Technology, Pasadena.
[2]Rutherford Appleton Laboratory, Oxfordshire, England.
[3]University of Virginia, Charlottesville.
[4]Heriot-Watt University, Edinburgh, Scotland.

Paper number 93JD00798.
0148-0227/93/93JD-00798$05.00

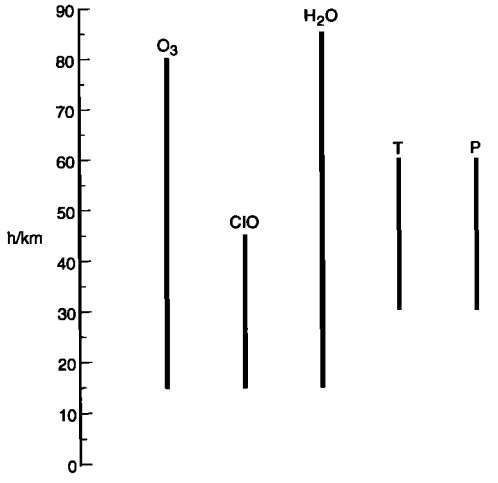

Fig. 1. Primary measurement objectives of Upper Atmosphere Research Satellite (UARS) microwave limb sounder (MLS). T is temperature and P is pressure.

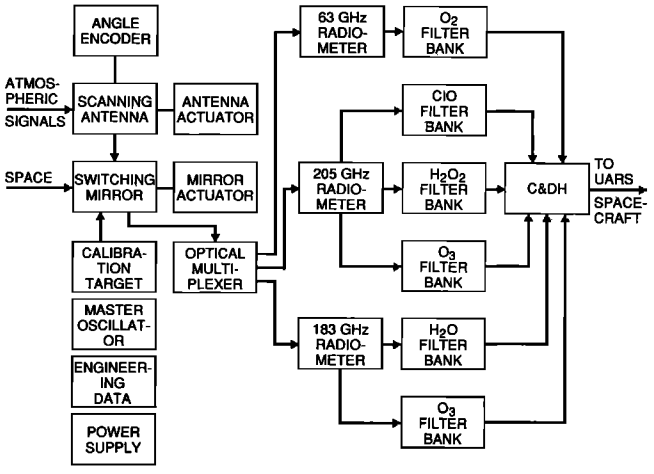

Fig. 2. MLS instrument block diagram.

internal target or a space view. A dichroic plate following the switching mirror separates a signal to the 63-GHz radiometer (for 62.998- and 63.569-GHz O_2 lines). A polarization grid then separates signals to the 183-GHz radiometer (for 183.310-GHz H_2O and 184.378-GHz O_3) and to the 205-GHz radiometer (for 204.352-GHz ClO, 206.132-GHz O_3, 204.575-GHz H_2O_2, and several weak lines of HNO_3).

Ambient-temperature Schottky-diode mixers downconvert the radiation to intermediate frequency (IF) bands in the range 0–3 GHz. The radiometers have approximately equal response at IFs above and below the local oscillator. The 183- and 205-GHz local oscillators are generated by frequency-tripling the outputs of phase-locked Gunn oscillators and are combined quasi-optically with the signals. The IF signals, after amplification, are further frequency-converted to six spectral bands, each centered at 400 MHz with a 510-MHz width. These bands are input to six filter banks which split the signal into 15 contiguous spectral channels, integrate the power received in each of these channels, and digitize the resulting signals for transmission to the ground. Spectral resolution of the individual filters is sufficient to resolve atmospheric emission lines throughout the stratosphere. (The instrument initially was designed to provide better resolution for mesospheric emission lines, but this was removed for financial reasons.) "Total power" measurements are made with an integration time of 1.8 s, and a vertical scan in discrete steps over the altitude range ~5–95 km is performed every 65 s. The scan tracks the Earth's limb by using "oblateness" signals generated by UARS to modify the scan pattern.

The instrument has three assemblies: spectrometer, power supply, and sensor. The overall mass is 283 kg, power consumption is 162 W, and output data rate is 1250 bits s^{-1}. Plate 1 is a photograph of the MLS sensor and spectrometer in flight configuration. A photograph showing MLS on the UARS observatory during ground testing at completion of thermal vacuum tests is given by *Waters* [1991]. Instrument subsystems and performance are described below.

ANTENNA

The antenna subsystem is a dual-offset Cassegrain consisting of three elliptical reflectors with characteristics given in Table 2. The primary is an offset paraboloidal section with a 1-m focal length; the hyperboloidal secondary forms an output beam whose focal length to diameter (f/D) ratio is dictated by the needs of the quasi-optical devices which combine signal and local oscillator for the 183- and 205-GHz radiometers; the flat tertiary diverts the limb radiation signal into the radiometer module. The optical beam axis out of the tertiary is coincident with the antenna mechanical scan axis.

The reflector surface precision is 28 μm root-sum-square (rss) over the three surfaces. The consequent upper bounds on scattering loss are 0.005 for the 63-GHz band, 0.043 for the 183-GHz bands, and 0.054 for 205 GHz. The actual losses are less because surface errors having large correlation length produce effects which are measured in the antenna patterns [*Ruze*, 1966] and thus accounted for. The

TABLE 1. Microwave Limb Sounder (MLS) Radiometers, Spectral Bands, and Primary Measurements

Radiometer	LO Frequency, GHz	Wavelength, mm	Band Designation	IF Range, MHz	Primary Measurement
1	63.283	4.74	B1	90–540	pressure temperature
2	203.267	1.48	B2	830–1340	ClO
			B3	1053–1563	H_2O_2
			B4	2610–3120	O_3
3	184.778	1.62	B5	1213–1723	H_2O
			B6	145–655	O_3

LO, local oscillator; IF, intermediate frequency.

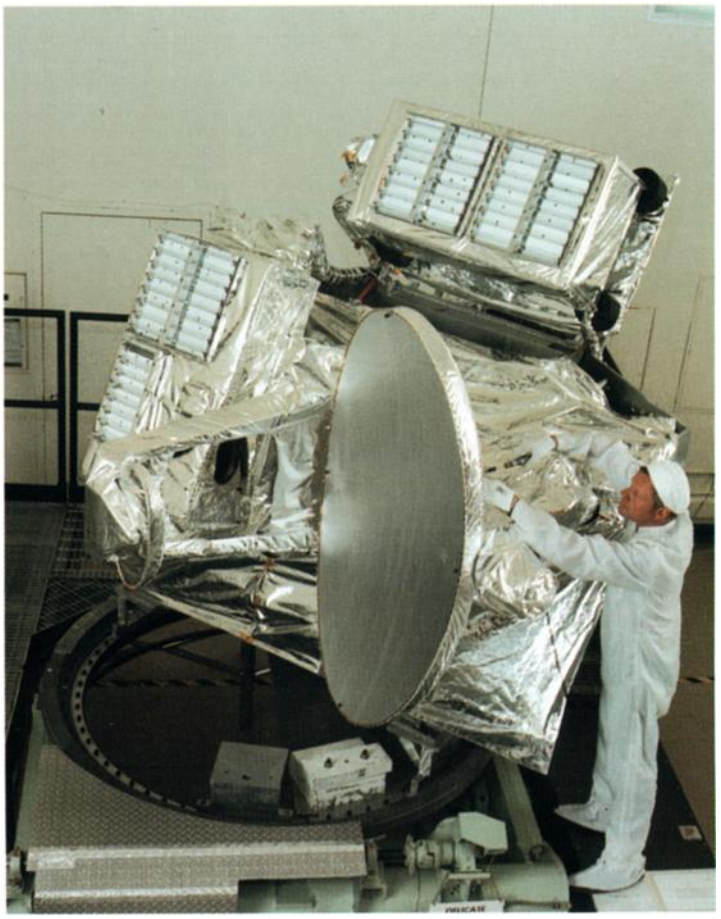

Plate 1. Photograph of the MLS instrument in-flight configuration on test stand.

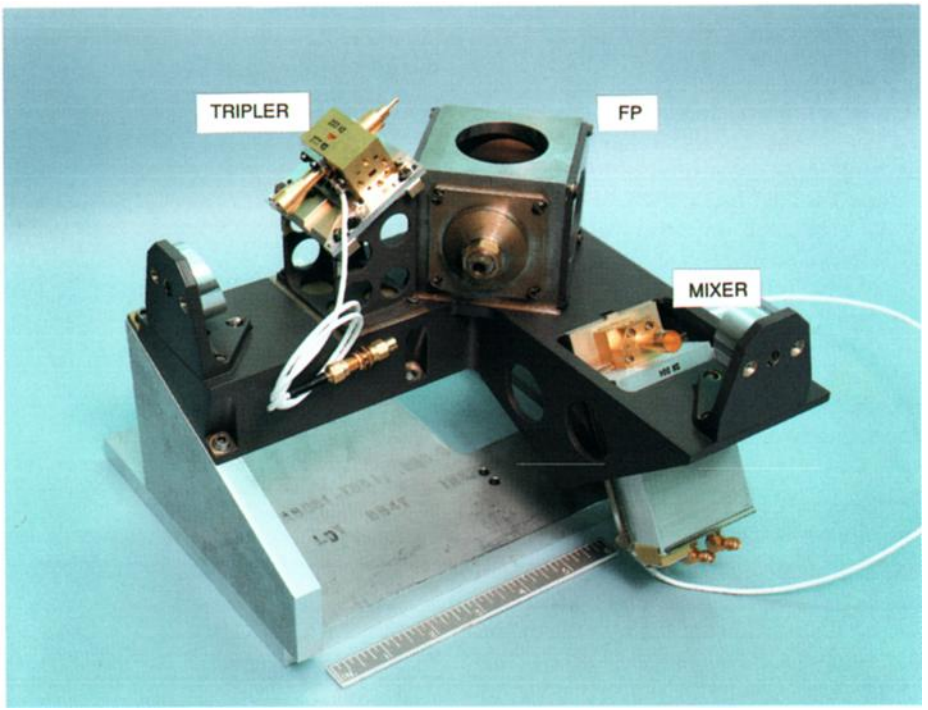

Plate 2. MLS 205-GHz receiver in-flight configuration.

TABLE 2. MLS Antenna Characteristics

Parameter	Primary	Secondary	Tertiary
Reflector size, m	1.6 × 0.8	0.45 × 0.24	0.24 × 0.20
Type	offset paraboloid	hyperboloid	flat
Effective focal length, m	5.9	5.9	∞
Surface accuracy, μm rms	23	13	8
Edge illumination, dB	−15	−20	−22

signal-to-noise ratio (SNR) achieved during antenna tests imposed a limit on this reduction. The SNR was 55 dB for 63-GHz patterns, 42 dB for 183-GHz patterns, and 50 dB for 205-GHz patterns, resulting in estimated scattering losses of 0.001, 0.012, and 0.008, respectively.

Antenna performance was verified by FOV calibration described below. Dependences of FOV pattern on scan angle and frequency within the RF bands were negligible. Table 3 summarizes the antenna subsystem performance. Performance of the antenna under orbital conditions was predicted using temperature fields from a thermal model in a NASTRAN structural analysis program which calculated deformations. In turn, these calculated deformations were used as inputs to an optics model. Predicted changes in pointing direction and aperture phase curvature were well within allowances for all anticipated temperature conditions. Bead blasting in the final stages of manufacture gave the reflectors their required thermal radiative properties.

Optical Multiplexer

The optical multiplexer separates the radiation from the switching mirror into the three radiometers, as illustrated schematically in Figure 3, which also shows block diagrams of the three MLS radiometers. It has low signal path losses, ranging from 1.0 to 1.5 dB, and also provides beam shaping to match the elliptical beams from the antenna to the circular patterns of the radiometer feed horns. Gaussian beam design techniques [e.g., *Goldsmith*, 1982] were used.

The 63-GHz beam is separated using a dichroic plate consisting of equispaced circular holes in a λ/4 metal plate. The 183- and 205-GHz beams are separated by a polarization grid of finely spaced wires. The signals are coupled to the symmetrical receiver feed horns using toroidal focusing mirrors. Stray radiation is controlled using RF absorbing paint within the multiplexer, augmented on critical areas by the iron-loaded epoxy absorber used in the calibration target.

Radiometer FOV patterns, relative responses of the radiometer assembly to signal as a function of angle, were measured to verify alignment, proper coupling to the antenna, and spillover levels. Knowledge of relative pointing between radiometers was verified to 2 arcsec with antenna pattern measurements using two nearly coincident transmitters.

Radiometers

The 205-GHz mixer is a single-ended fundamental mount based on the design by *Archer and Mattauch* [1981]. Combined signal and local oscillator (LO) are fed into the mount by a modified Potter dual-mode feed horn [*Potter*, 1963; *Pickett et al.*, 1984]. The GaAs Schottky diode (University of Virginia Semiconductor Devices Laboratory, type 1H20) used in the mixer has a DC series resistance of 6.5 Ω and a zero bias capacitance of $3.5\,fF$. It is soldered to a 76-μm-thick quartz dielectric microstrip RF choke and contacted by a 100-μm-long, 6-μm-diameter phosphor bronze whisker. The 1.3-mm-long choke is a high-impedance/low-impedance low-pass filter in which the diode forms the first capacitive section. The IF port of the mixer is matched to 50 Ω and then diplexed into two IF bands, one from 830 to 1580 MHz for the ClO/H_2O_2 bands and the other from 2610 to 3120 MHz for the O_3 band. The diplexer uses complementary Chebyshev high- and low-pass filters. The matching network and diplexer are integral with the mixer mount to reduce loss. The insertion loss in the low-pass path of the diplexer is less than 0.3 dB and less than 0.7 dB in the high-pass arm.

The LO is a phase-locked Gunn diode oscillator driving a crossed-waveguide frequency tripler. The tripler is a modification of the *Archer* [1981] design. The nonlinear element is a GaAs Schottky varactor (University of Virginia, type 6P4) and has a zero bias capacitance of $21\,fF$, a DC series resistance of 11 Ω, and reverse bias breakdown of 16.5 V. The Gunn output is coupled into full height WR 15 waveguide to a 76-μm quartz suspended strip line low-pass filter with a 3-dB cutoff frequency of 115 GHz, passing the input frequency but rejecting both the doubled and the tripled frequencies. The whisker-contacted varactor diode is soldered to the end of the quartz dielectric in the reduced height output waveguide. The output waveguide consists of a cavity that supports the fundamental modes at both the doubled and the tripled frequencies. The cavity extends about half a wavelength for the doubled frequency from the diode, providing a short at the diode. Beyond the idler cavity is the output waveguide which is cut off at the doubled

TABLE 3. Antenna Subsystem Performance

Parameter	B1	B2, B3, B4	B5, B6
Vertical HPBW,*°	0.206	0.064	0.077
Vertical HPBW at tangent point, km	9.5	3.0	3.6
Horizontal HPBW,°	0.43	0.145	0.152
Hortizontal HPBW at tangent point, km	20.3	6.8	7.2
Beam efficiency	0.91	0.90	0.91
Peak cross polarization, dB	−30	−19	−20
FOV elevation direction knowledge,°			
absolute, B1 to alignment cube	0.0036		
relative to B1		0.0016	0.0021
Ohmic efficiency†	0.992	0.989	0.992
Wide-angle efficiency‡	0.931	0.976	0.977

*HPBW, half power beam width.
†Ohmic efficiency, 1 − ohmic loss.
‡Modeled, including spillover, scattering and edge diffraction.

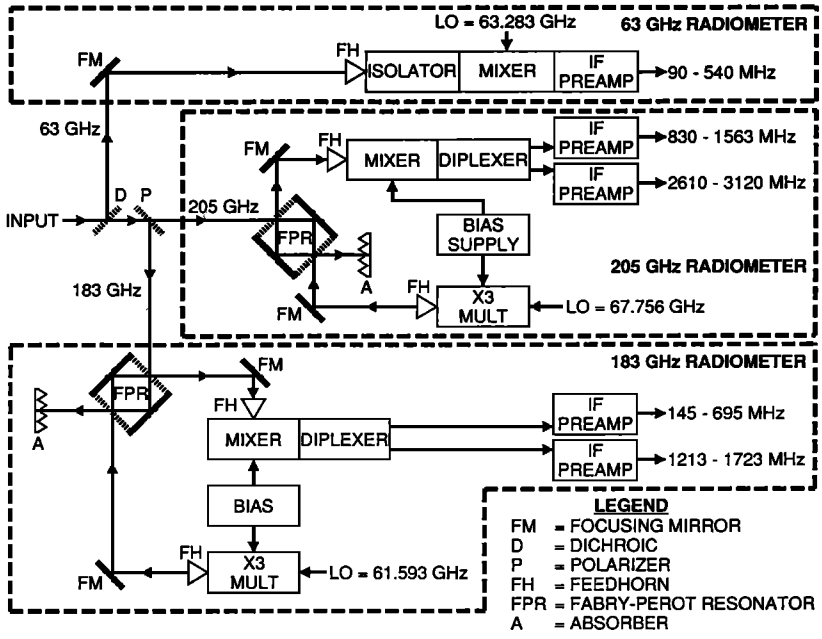

Fig. 3. Radiometer block diagrams.

frequency but transmits the tripled frequency. A dual concentric circular backshort tunes both the idler and the output frequencies. Tripler efficiency is ~6%.

The signal and LO are combined in a folded Fabry-Pérot (FP) ring resonator based on a design by *Gustincic* [1977] and modified by *Pickett and Chiou* [1983]. The broadband input signal is reflected off the FP resonator with very low loss, while the monochromatic LO signal is transmitted through the tuned cavity with minimal loss. Transverse modes are suppressed by absorbing baffles within the cavity. The ring resonator is constructed of Invar to maintain alignment over the operating temperature range.

Steps were taken to insure that the mixer and tripler, whose design had not previously been flown in space, would survive the launch and space environment. The whisker post was epoxied in place, rather than relying on friction as is conventional for ground-based systems. The whisker diameter was reduced to 6 μm, significantly decreasing its spring constant, allowing increased longitudinal compression with consequently greater stability. Diodes with deep wells (0.7 μm) to hold the whisker in place laterally were specially developed at the University of Virginia.

Each mixer diplexer IF output is routed to a multistage low noise preamplifier through semirigid coaxial cable. The preamplifiers are compact space-qualified commercial modules utilizing standard IF design and construction techniques.

The radiometer performance is summarized in Table 4; further design details are available in the work of *Frerking et al.*, [1983]. Plate 2 shows a photograph of the 205-GHz radiometer.

The 183-GHz radiometer is functionally the same as the 205-GHz radiometer with only minor differences. The most significant are a modified FP mesh hold-down technique, a different diplexer arrangement to yield the required IF outputs, and a modified approach to the implementation of the LO phase-lock electronics. The performance is summarized in Table 5.

The 63-GHz radiometer is a space-qualified commercial

TABLE 4. Radiometer Performance, 205 GHz

	205-GHz Radiometer	
RF signal sideband frequency range, GHz	204.1–206.4	
Tripler output (LO) frequency, GHz	203.267	
Tripler input frequency, GHz	67.756	
Tripler output (LO) power, mW	2	
Tripler input power, mW	35	
	ClO/H_2O_2 Band	O_3 Band
DSB radiometer noise temperature, K	990	1530
DSB mixer noise temperature, K	620	800
Mixer conversion loss, dB	6	6
IF frequency range, MHz	830–1563	2610–3120
First IF amplifer noise figure, dB	<1.5	<2.0

TABLE 5. Radiometer Performance, 183 GHz

	183-GHz Radiometer	
RF signal sideband frequency range, GHz	182.7–184.5	
Tripler output (LO) frequency, GHz	184.778	
Tripler input frequency, GHz	61.593	
Tripler output (LO) power, mW	2.5	
Tripler input power, mW	45	
	H_2O Band	O_3 Band
DSB radiometer noise temperature, K	1650	1820
DSB mixer noise temperature, K	900	900
Mixer conversion loss, dB*	7.5	7.5
IF frequency range, MHz	1213–1723	145–655
First IF amplifer noise figure, dB	<2.0	<2.0

*Including integral IF diplexer loss.

TABLE 6. Radiometer Performance, 63 GHz

	63-GHz Radiometer
RF double sideband frequency range, GHz	62.5–64.0
LO frequency, GHz	63.283
DSB radiometer noise temperature, K	400
IF frequency range, MHz	90–540

mixer-amplifier module utilizing a balanced pair of packaged Schottky barrier diodes in a fundamental mixing mode. The input signal path comprises of focusing mirror, a modified Potter feedhorn, and a waveguide isolator. The local oscillator is a phase-locked Gunn coupled into the mixer by waveguide. The performance is summarized in Table 6.

INTERMEDIATE FREQUENCY

The intermediate frequency (IF) subsystem provides amplification of the signals from the mixer-IF preamplifiers and conversion to a 400-MHz center frequency for input to the filter banks. There are six IF chains: one for the 63-GHz radiometer (B1), three for the 205-GHz radiometer where the ClO/H_2O_2 band from the diplexer is further subdivided into two bands (B4, and B2 and B3), and two for the 183-GHz radiometer (B5 and B6). Figure 4 shows the IF frequency ranges and the local oscillators. The frequency response of each chain is set by band-pass filters. The gains are set by variable attenuators controlled by the control and data handling (C&DH) subsystem which also monitors the gain control settings and temperatures in each module. Each IF is in a separate subchassis and uses microstrip circuits and commercial mixer, filter, and amplifier microwave integrated circuit (MIC) modules. Performance characteristics are summarized in Table 7.

An IF switching network is installed between the IF outputs and the filter banks. It allows, by C&DH command, simultaneous connection of two filter banks to any of the six IF outputs. This provides redundancy for the critical measurements should a filter bank fail and allows intercomparison of filter bank characteristics.

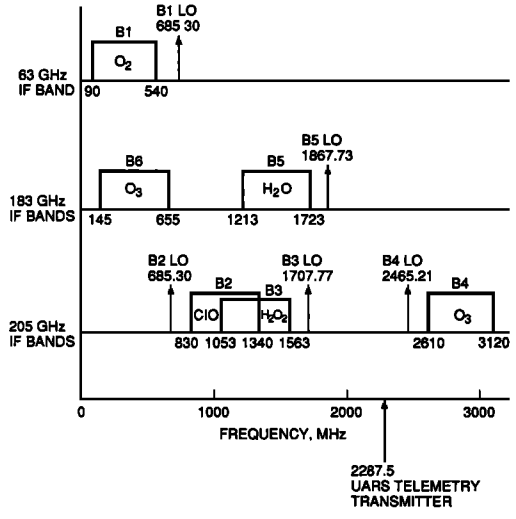

Fig. 4. Intermediate frequency (IF) spectrum. Second local oscillator (LO) frequencies are indicated.

TABLE 7. IF Subsystem Characteristics

	IF Subsystem
Bandpass ripple, dB	±1.5
Nominal gain, dB	+30
Gain control range, dB	>30
Nominal output power, dBm	−9
Output power at 1 dB gain compression dBm	+8
Noise figure, dB	10 to 17
Image rejection, dB	≥25
Input VSWR	<2:1
Output VSWR	<2:1
Temperature gain coefficient, % per °C	<1.0

FILTER BANKS

The six filter banks are identical in design and construction. The 400-MHz IF input from the radiometer is split into 15 channels through a series of power splitters and band-pass filters. Amplification is provided to compensate for channelization losses. Channel center frequency and bandwidth, shown in Table 8, are achieved by two types of filters: discrete-element Chebyshev LC filters with 10 or 12 poles for the 32-MHz to 128-MHz channels and quartz surface acoustic wave (SAW) filters for the 2- to 16-MHz-wide channels. Temperature-insensitive back diode detectors convert the filtered signal to a proportional DC voltage. These voltages are amplified, then integrated by voltage-to-frequency (V-to-F) converters and 16-bit counters.

The detector diodes and RF amplifiers are operated at signal levels which maintain overall linearity to better than 1 part in 1000 [*Jarnot and Cofield*, 1991]. In addition, the digitizers were designed to allow integration down to well below the 1-bit level without introduction of systematic errors.

LOCAL OSCILLATORS

The local oscillator subsystem provides frequency-stable local oscillators for the radiometers and the clock for the C&DH subsystem. All signals are derived from a high-stability quartz crystal oscillator through frequency synthesis using phase-locked loops. The subsystem can also accept an external signal so that the frequencies of the first local oscillators can be offset to compensate for the index of refraction of air and thereby allow correct operation of the Fabry-Pérot local oscillator diplexers during ground testing. The frequency is stable to one part in 10^7 for all combinations of environmental and electrical conditions after final ground calibration through to the end of the mission. A block diagram of the local oscillator subsystem is given in Figure 5.

The local oscillator frequencies were established to within approximately 10 MHz by the scientific requirements that (1) no atmospheric spectral lines appear within the mixer image sidebands which might interfere with the primary measurements and that (2) the O_2 lines measured by the 63-GHz radiometer overlay each other in the IF passband. Further constraints required that no IF passbands contain the UARS telemetry transmitter frequency, that no harmonics of any internal frequency should appear in any spectral passband, that all downconversions must result in line centers within 200 kHz of a common filter bank center frequency, and that all local oscillator frequencies must be simple rational fractions of a common reference frequency. A computerized

TABLE 8. Filter Bank Characteristics

Channel	Filter Type	Center Frequency, MHz		3 dB Bandwidth, MHz		*R* Value,* %
		Nom†	Actl‡	Nom†	Actl‡	
1	LC	209	209.3	128.0	126.0	94.5
2	LC	305	305.8	64.0	64.0	93.2
3	LC	353	353.4	32.0	31.3	91.7
4	SAW	377	377.2	16.0	15.8	95.2
5	SAW	389	389.2	4.0	3.8	93.5
7	SAW	398	398.1	2.0	1.9	89.0
8	SAW	400	400.0	2.0	2.0	89.3
9	SAW	402	402.1	2.0	2.0	89.7
10	SAW	405	404.9	4.0	3.9	93.5
11	SAW	411	410.7	8.0	7.8	94.7
12	SAW	423	423.3	16.0	15.6	95.2
13	LC	447	448.4	32.0	32.3	90.1
14	LC	495	494.8	64.0	62.5	91.2
15	LC	591	592.0	128.0	128.1	94.7

*R value defined as percent of spectrally flat power received within 3-dB bandwidth.
†Nominal.
‡Actual for one filter bank; all others similar.

search revealed three candidate base frequencies between 700 kHz and 1 MHz. The chosen base frequency had the smallest maximum prime number in its sequence of frequency synthesis ratios. The sixth harmonic of this base frequency, 4.704 597 924 MHz, was also close to the common low-drift quartz crystal oscillator frequency standard frequency of 5 MHz and therefore was selected as the MLS master oscillator frequency.

CONTROL AND DATA HANDLING (C&DH)

The C&DH is a microprocessor-based (NSC800) system with 4 kB of fusible link PROM and 12 kB of radiation-hardened static RAM. It provides bidirectional communication with UARS via a remote interface unit (RIU) and with the filter bank, engineering data, control, and scan electronics subsystems via a 1-bit serial bus which multiplexes both commands and data. A differential configuration is used for the serial bus to eliminate ground loop problems. Each subsystem has a unique address, and the subsystem interfaces are designed to allow any power supply or single component failure to occur without impacting bus traffic. All operation of the C&DH is programmable and includes the ability to entirely reprogram the system from the ground. In addition to ground control of many instrument-operating parameters, the C&DH accepts an oblateness command from UARS. This command provides information on the Earth's oblateness at the MLS FOV tangent point and is used to dynamically modify the antenna scan pattern to track the atmospheric limb.

Engineering data are digitized using the same V-to-F converter design as in the filter banks, affording high-resolution temperature (0.002 K) and voltage (10 μV) telemetry. Analog engineering data are multiplexed into six 16-bit telemetry words, each of which cycles through 32 parameters in 65.536 s, the engineering major frame rate of UARS. Internal subsystem calibration is provided by periodic measurement of internal precision voltage and resistance references. The order in which parameters are digitized may be set by ground command for diagnostic purposes.

The radiometer control subassembly provides analog control signals (12-bit resolution) to the mixer and multiplier bias units, the IF gain control units, and the 183 Gunn phase-lock system. Additional digital outputs are provided to the 63- and 205-GHz Gunn phase-lock systems for bias control and to all Gunn phase-lock systems for loop closure control. Recovery from single-event upset conditions is provided by continuous C&DH refresh of all radiometer control internal registers.

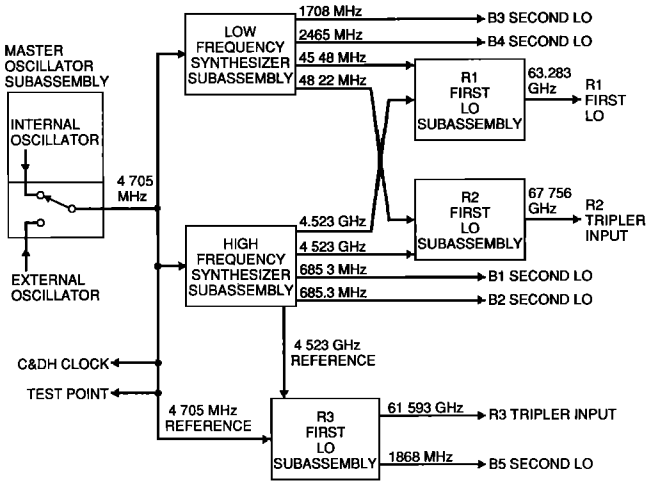

Fig. 5. MLS local oscillators block diagram.

MECHANISMS

Support and pointing of the 40-kg antenna subsystem is by bearings at either side of the primary. It is scanned by a linear actuator arranged as an off-axis strut. The bearings employ grease-lubricated, sealed spherical roller units which were selected for their large load capacities, low friction, and insensitivity to structural and thermal deflections. The linear actuator is a ball-screw unit driven by a permanent magnet stepper motor. The inherent stiffness and high load-carrying capacity of the ball-screw unit make it well suited for this application. A stroke of 78 mm produces 9.2° rotation of the

antenna; a rotation of 0.0025° is achieved for each motor step. Antenna position is measured to relative accuracy of 1.8 arcsec by a 19-bit resolution incremental optical shaft angle encoder mounted at one end of the antenna support structure. The switching mirror is supported on the output shaft of a motor actuator, a brushless permanent magnet stepping motor with a 1.0° step size. Step time is 200 ms (for 102° rotation) with position repeatability of 0.05°.

MECHANICAL AND THERMAL DESIGN

Sensor Structure

The MLS sensor structure consists of the reflectors, the antenna structure, and the support structure. The antenna structure supports the three reflectors and allows for scanning about one axis. The reflectors and antenna structure are made of the same material to maintain alignment during temperature variations in orbit. Aluminum was chosen to reduce cost.

The primary reflector front face sheet thickness of 1.7 mm provides thermal uniformity and allows for possible final machining to achieve the required surface accuracy of better than 25 μm. The front and rear face sheets were stretch-formed over a mandrel, and the honeycomb sandwich was laid up over a form, vacuum-bagged during bonding, and then postcured. No postfabrication machining was required. Fabrication of the secondary was similar. The tertiary is made of 40-mm-thick flat honeycomb.

The antenna structure consists of a pair of aluminum arms machined to a C-shaped cross section with a cover sheet to make a hollow box-beam. These arms incorporate the scan bearings and mounting pads for the reflectors. The support structure provides the scan axis alignment, radiometer module mounting, and spacecraft interface. To accommodate the statically determinate three-point mounting on the spacecraft and a 35-Hz minimum natural frequency requirement, the support structure includes a large, torsionally rigid tube connecting the two scan-axis bearing supports.

Electronics Packaging

The instrument electronics are packaged into three separate machined housings: the radiometer module, the spectrometer assembly, and the power supply assembly. Electronic components are mounted on single or multilayer printed circuit boards, with all electronic components surface mounted. The boards are attached to shear plates which provide additional rigidity to the assemblies in which they are mounted. Sensitive electronics are mounted into shielded subchassis.

Thermal Design

The thermal control system accommodates all thermal environments from ground operation through orbital operation. The design includes (1) maximum isolation from solar heating using multilayer insulation (MLI) with a solar reflective surface finish; (2) multilayer insulation on shaded surfaces to minimize gradients and heat losses; (3) heat rejection at electronic bay surfaces primarily by radiators; (4) radiator surfaces with active louvers to minimize survival power requirements; (5) maximum internal conductive coupling to suppress gradients; (6) passive antenna thermal control that relies on thermal radiative and conductive properties, MLI, thermal capacitance, and shading from the Sun by the spacecraft; and (7) maximized thermal isolation between the instrument and the spacecraft with the intent of making instrument and spacecraft thermal designs as independent as possible.

The thermal design was carried out analytically by means of thermal mathematical models. A thermal balance test [*Siebes*, 1989] was performed on the PFM in a vacuum chamber to verify these models and to validate the thermal control system.

INTEGRATION, TEST, AND VERIFICATION

The integration, test, and verification program constituted a comprehensive system level demonstration that the MLS could make measurements of atmospheric emissions with the accuracy needed for retrieval of the desired geophysical parameters. The testing had to show that the electrical, mechanical, and thermal interfaces to the spacecraft were correct, that the instrument could withstand the launch and in-orbit environments, and that its functional performance satisfied the design requirements. System level verification began with experiments on a brassboard model of the radiometer module and continued with more systematic tests on the fully functional vibration test model (VTM) of the sensor assembly. During the integration, test, and verification program at Jet Propulsion Laboratory (JPL) the MLS instrument was operated for more than 1700 hours, and an additional 800 hours were added during spacecraft integration and prelaunch tests. Engineering and performance data obtained from standard instrument functional test runs throughout this period showed no significant trends.

CALIBRATION

Radiometric Calibration

Prelaunch radiometric calibration consisted of (1) determining the performance of the internal calibration target; (2) verifying the linearity of the system transfer function ("counts" out of the spectrometer channels versus power in); and (3) determining the optical losses "in front of" the switching mirror.

The switching mirror provides routine radiometric calibration by directing all radiometer FOVs to views of "cold space" and an internal ambient blackbody calibration target. An algorithm which produces optimum estimates (in terms of signal to noise) of interpolated reference and target signals has been developed [*Peckham*, 1989] and applied to the MLS radiometric calibration.

The calibration target emissivity was determined by measuring the reflected signal from a transmitter at varying angles of incidence: emissivity >0.9998 was inferred for all bands. System linearity was verified by measuring channel response when switching between temperature-controlled targets (of the same type as the calibration target) on the limb and space ports of the radiometer module. Optical properties and losses were determined as part of the FOV calibrations (described below).

Spectral Calibration

There are two major areas of spectral calibration: (1) measuring the frequency response of the individual filter

channels through the entire signal chain (antenna input to filter bank output) and (2) determining the relative sideband response in each channel.

The individual channel responses were measured using a synthesized frequency source with a cesium frequency standard as its reference. This equipment was also used to confirm there were no unwanted instrumental responses throughout the band.

Relative sideband response was measured by viewing through a scanning plane Fabry-Pérot to alternately observe blackbody targets at ambient and liquid nitrogen temperatures. These measurements also assured the absence of unwanted harmonic or subharmonic mixer responses.

Field-of-View (FOV) Calibrations

FOV calibrations included (1) antenna FOV pattern measurements at several frequencies in each radiometer passband, at several angles within the scan range, in both polarizations in several planes; (2) radiometer-to-radiometer relative boresight determination and absolute boresight determination of the 63-GHz radiometer FOV (the pointing reference radiometer) with respect to the UARS optical reference cubes; (3) measurement of radiometer patterns to determine beam truncation at each aperture of the radiometer (required for radiometric calibration) and to verify design antenna illumination; (4) determination of antenna system losses and of pickup due to stray radiation; and (5) development of models which predict pointing variations as a function of hardware temperature fields and flag conditions under which predictable background radiance contamination could occur.

Antenna pattern measurements were performed using frequency-locked transmitters as the signal sources. The patterns were characterized on far-field ranges at 3 and 1 km, at 10 scan angles, and ~5 frequencies within each band. Boresight directions (dFOV) at 63 and 205 GHz were measured with accuracy of 15 arcsec relative to a sensor alignment cube using a theodolite.

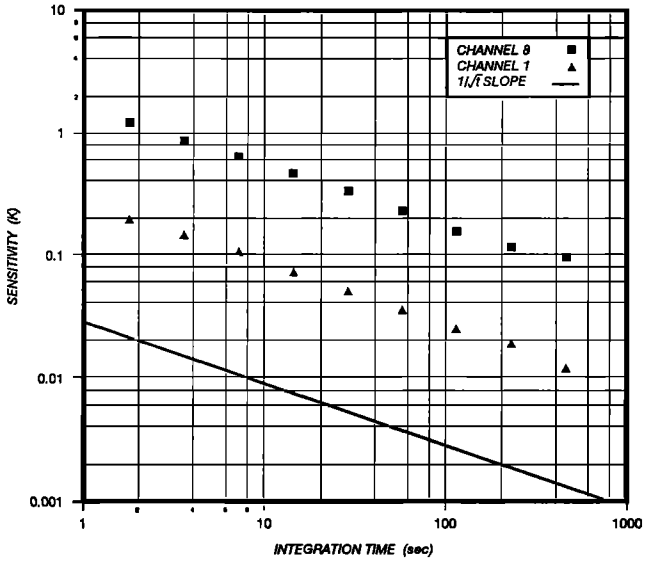

Fig. 6. Radiometric sensitivity (K) versus integration time (s) for channel 1 (128-MHz bandwidth) and channel 8 (2-MHz bandwidth) of band 2 (ClO). Solid line indicates a slope of (integration time)$^{-1/2}$

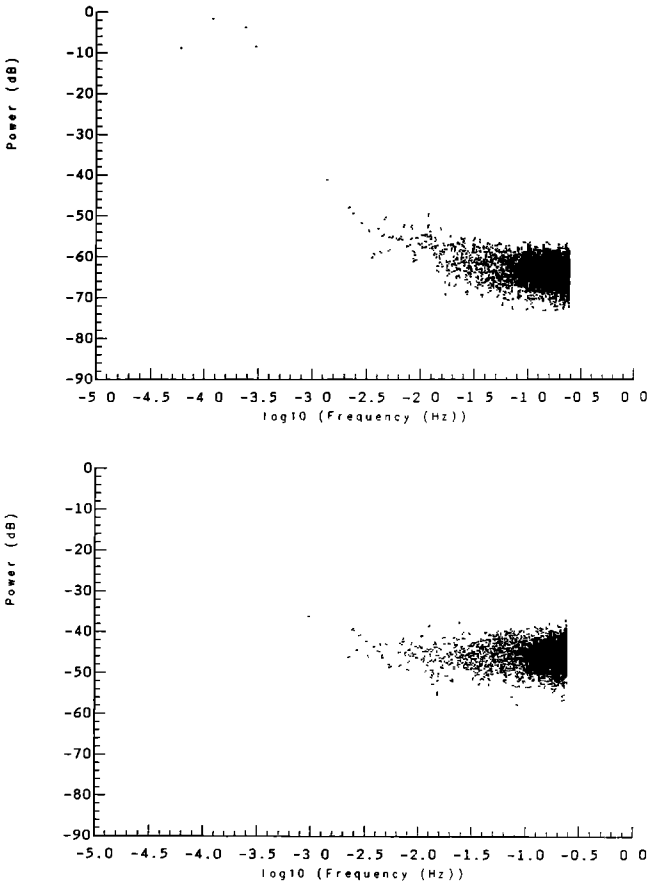

Fig. 7. Noise power spectrum for channel 1 (top) and channel 8 (bottom) of band 2, computed from 8192 consecutive 2-s observations of the MLS internal calibration target.

The calibrations were performed to an accuracy which when combined with postlaunch characterization data and ground truth measurements should provide measurement of O_3 to better than 3% accuracy, with a goal of 1%.

Long-Term Calibration Stability

The long-term resiliency of prelaunch calibrations was verified by specific tests. Samples of each filter type (LC and SAW) used in the filter banks were life-tested over a 3-year interval which included periodic temperature cycling and operation at elevated temperatures. No statistically significant changes in filter performance were observed. Sideband response sensitivity to mixer bias (AC and DC) was investigated and revealed an insignificant sensitivity to LO drive until LO power had decreased to 50% of its prelaunch value. Slight dependence of sideband ratio on DC bias was observed, and hence the mixers are being biased in orbit at their prelaunch levels. Both mixer and multiplier bias levels are monitored with high resolution and are ground commandable to compensate for any future aging effects. FOV response is highly sensitive to mechanical alignment, and the integrity of the MLS design was verified by performing full FOV characterization on the VTM before and after vibration testing. No changes were observed. In addition, mechanical alignment of the flight antenna system was periodically

TABLE 9. Radiometric Noise for Space View Measurements

Band	Radiometric rms Noise for Single Integration, 1.8 s, K		Radiometric rms Noise for 150 Integrations, 4 min, K	
	Wing Channel, BW = 128 MHz	Center Channel, BW = 2 MHz	Wing Channel, BW = 128 MHz	Center Channel, BW = 2 MHz
1	0.03	0.21	0.002	0.017
2	0.13	1.04	0.011	0.085
3	0.14	1.09	0.011	0.089
4	0.20	1.61	0.016	0.132
5	0.22	1.74	0.018	0.142
6	0.24	1.92	0.020	0.157

*The typical integration time for MLS daily zonal mean data products is 4 min.

verified via a set of tooling balls built into the assembly. Further instrument calibration details are available in the work of *Jarnot and Cofield* [1991].

PERFORMANCE

The radiometer noise temperatures, given in earlier sections for each of the MLS bands, and the radiometric sensitivity given in Table 9, are primary indicators of the instrument noise. An extremely important requirement is to reduce noise by averaging individual measurements. Prelaunch tests by using long (24 hours) data sets taken with the instrument viewing the internal calibration target confirmed this requirement was met. Figure 6 gives typical results from such a test and shows that data can be averaged for up to at least 500 s with noise decreasing inversely with the square root of time. Similar performance is being achieved in orbit, with repeatability at ~0.01 K as demonstrated by daily zonal averages of radiance spectra when observing cold space.

The power spectra of outputs from individual channels taken when viewing a stable reference for an extended period of time provide an indicator of stability. Figure 7 shows such data for a 128-MHz and 2-MHz bandwidth channel (upper and lower section of the figure, respectively). The noise power is seen to be predominantly Gaussian (spectrally flat) at high frequencies but increases at approximately $1/f$ at lower frequencies, typical for a system of this type. The breakpoint frequency (intersection of the $1/f$ and spectrally flat regions) for the wide channel occurs at a

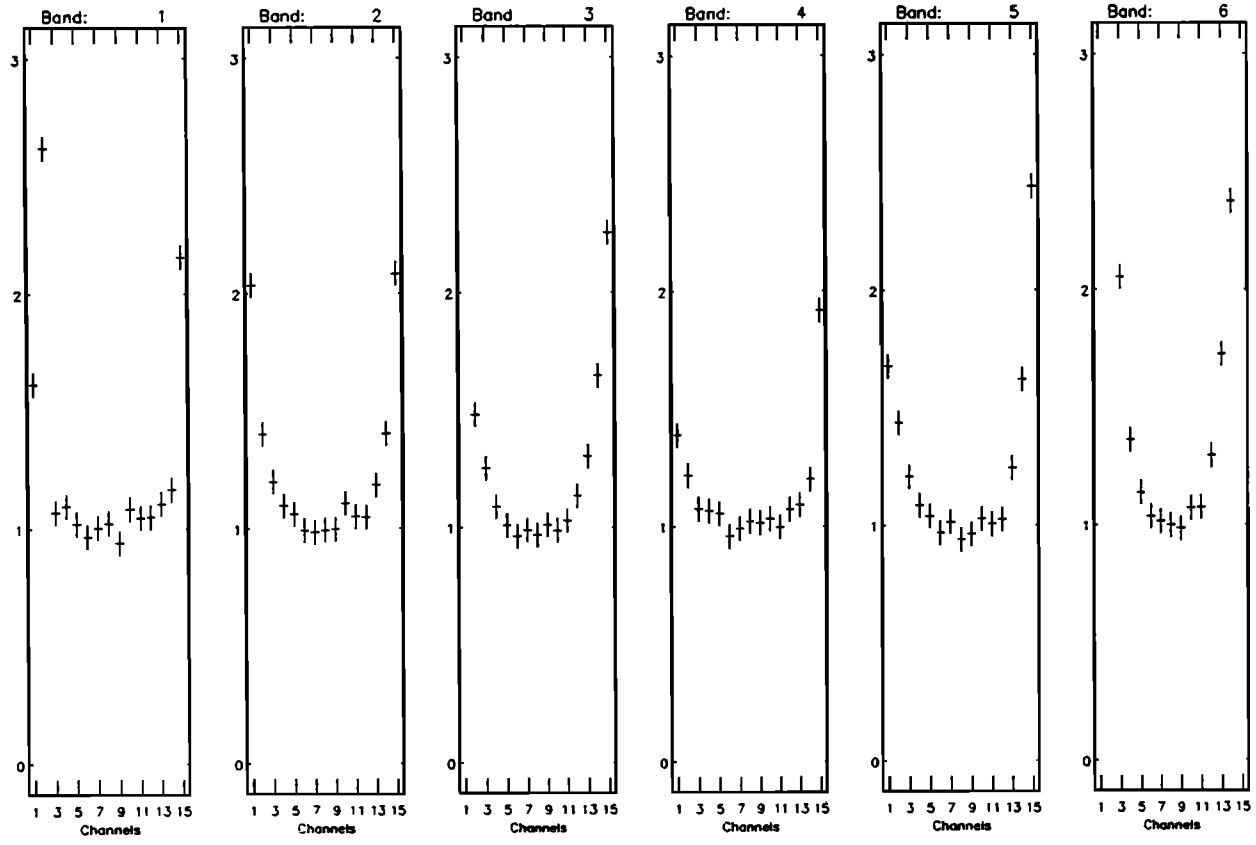

Fig. 8. Average χ^2 statistic for all 90 channels, computed from all views to space for 1 day. (A value close to 1 indicates that sensitivity for the channel is limited by radiometric noise; higher values show that sensitivity is degraded by $1/f$ noise.)

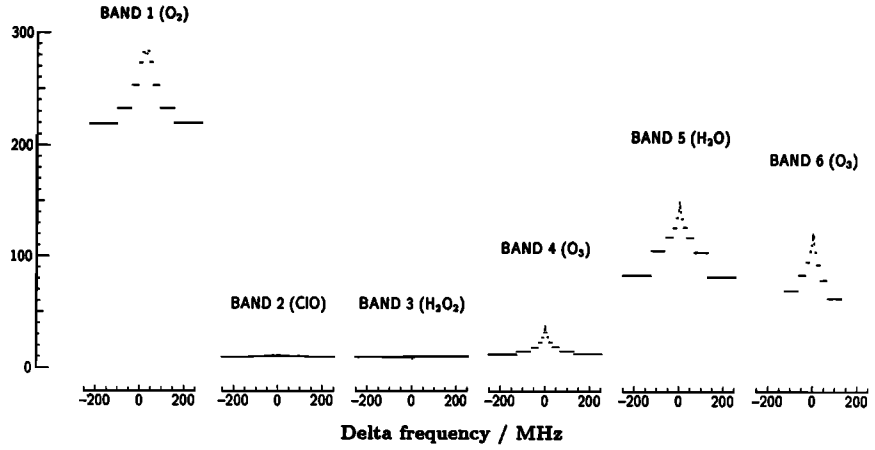

Fig. 9. UARS MLS spectra at 20-km tangent height.

higher frequency than for the narrower channel, as expected. For $1/f$ noise not to compromise data quality, it is necessary to perform calibrations at a rate commensurate with the $1/f$ breakpoint frequency. Intervals of 16.4 s for space views and 65.5 s for target views are currently implemented.

An indicator of S/N degradation caused by $1/f$ noise is provided by evaluation of the χ^2 statistic. Figure 8 shows the result of this computation for a full day of space views on October 24, 1991. A value of unity, typical for most channels, indicates that S/N is dominated by radiometer noise. The value of χ^2 rises slightly as channel bandwidth increases but represents only a minor degradation in S/N. These data indicate the advantage of total power measurements as implemented in the MLS; little to no loss in S/N is incurred in limb signal integrations when using ~20% of the observation time for calibration and reference views, rather than the ~50% of a conventional Dicke switched system. The χ^2 plots are generated daily for continuous performance monitoring, and the results in Figure 8 are typical. In-orbit $1/f$ characteristics are slightly better than indicated by ground-based measurements. This is expected because of the lower operating temperatures and improved thermal stability.

The instrument has been operating continuously throughout the first 16 months of the mission with no engineering problems or significant trends. On spacecraft yaw days, diagnostic engineering and calibration tests are conducted, and any required updates to the scan programs are performed. At all other times the instrument operates autonomously.

Figure 9 shows sample spectra for a single 1.8-s integration. These spectra were obtained on September 21, 1991, with the instrument FOV directed at ~20-km tangent height over the Antarctic Weddell Sea. The spectral lines of O_2, O_3, and H_2O are readily evident in this figure; the "inversion" in the center of the O_2 line is due to the center of that line sensing the colder mesospheric temperatures. The right-hand plot of Figure 10 shows the same ClO spectrum as in Figure 9 with the vertical scale expanded by a factor of 100. This illustrates that a single 1.8-s instrument integration provides good measurement of the enhanced ClO abundances in the Antarctic "ozone hole" when this spectrum

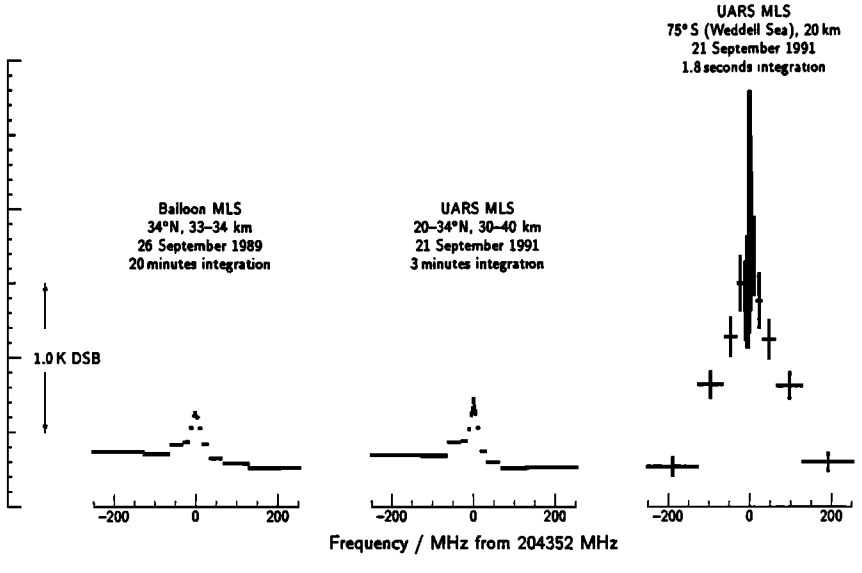

Fig. 10. Thermal emission by stratospheric ClO at 205 GHz.

was obtained. The middle spectrum in Figure 10 is a ClO zonal mean of upper stratosphere signals at mid-latitudes. The small "knee" on the left side of the upper stratospheric ClO line is due to a weak isotopic ozone line, and the slope upward to the left is due to a $H_2^{18}O$ line outside the spectral range of the filter bank. The leftmost spectrum in Figure 10 was measured by the balloon MLS (R. A. Stachnik, private communication, 1989) under conditions similar to that of the UARS MLS spectrum in the middle. Agreement between the balloon and the UARS MLS measurements is excellent.

Acknowledgments. We thank our many colleagues at the Jet Propulsion Laboratory, Rutherford Appleton Laboratory, and Heriot-Watt University who contributed to the MLS development. We are grateful to John Houghton for first proposing UK involvement in MLS, and to Peter Curtis for managing this involvement during critical early phases. UARS project personnel of the NASA Goddard Space Flight Center, especially Peter Burr and John Donley, are acknowledged for their excellent management of UARS and support of MLS. Personnel of the General Electric Corporation are also acknowledged for their support during integration and testing of MLS on UARS. The portion of this work performed at the Jet Propulsion Laboratory, California Institute of Technology, was under contract with the U.S. National Aeronautics and Space Administration. Work performed at the Rutherford Appleton Laboratory and Heriot-Watt University was supported by the U.K. Science and Engineering Research Council and the British National Space Center.

REFERENCES

Archer, J. W., Millimeter wavelength frequency multipliers, *IEEE Trans. Microwave Theory Tech.*, *MTT-29*, 552–557, 1981.

Archer, J. W., and R. J. Mattauch, Low noise, single-ended mixer for 230 GHz, *Electron. Lett.*, *117*, 180–181, 1981.

Frerking, M. A., J. C. Hardy, W. J. Wilson, and P. A. Zimmerman, Broadband low noise 205 GHz radiometer for a satellite receiver, *IEEE MTT-S Int. Microwave Symp. Dig.*, 110, 1983.

Goldsmith, P., Quasi-optical techniques at millimeter and submillimeter wavelengths, in *Infrared and Millimeter Waves*, vol. 6, *Systems and Components*, pp. 277–343, Academic, San Diego, Calif., 1982.

Gustincic, J. J., A Quasi-optical receiver design, *IEEE-MTT-S Int. Microwave Symp. Dig.*, 99–101, 1977.

Jarnot, R. F., and R. E. Cofield, Microwave limb sounder (MLS) instrument calibration report, *JPL Doc. D-9393*, August 1991.

Peckham, G. E., An Optimum calibration procedure for radiometers, *Int. J. Remote Sens.*, *10*, 227–236, 1989.

Pickett, H. M., and A. E. Chiou, Folded Fabry-Pérot quasi-optical ring resonator diplexer: Theory and experiment, *IEEE Trans. Microwave Theory Tech.*, *MTT-31*, 373–380, 1983.

Pickett, H. M., J. C. Hardy, and J. Farhoomand, Characterization of a dual-mode horn for submillimeter wavelengths, *IEEE Trans. Microwave Theory Tech.*, *MTT-32*, 936–937, 1984.

Potter, P. D., A new horn antenna with suppressed sidelobes and equal bandwidths, *Microwave J.*, 71, June 1963.

Reber, C. A., The Upper Atmosphere Research Satellite (abstract), *Eos Trans. AGU*, *71*(51), 1867–1878, 1990.

Robbins, D., et al., Ozone measurements from the Balloon Intercomparison Campaign, *J. Atmos. Chem.*, *10*, 181–218, 1990.

Ruze, J., Antenna tolerance theory—A review, *Proc. IEEE*, *4*, 633–640, 1966.

Siebes, G., Microwave limb sounder (MLS) thermal balance test report, *JPL Doc. D-6756*, September 1989.

Waters, J., Microwave limb sounding of Earth's upper atmosphere, *Atmos. Res.*, *23*, 391–410, 1989.

Waters, J., Submillimeter heterodyne remote sensing of upper atmospheric gases, *Microwave Opt. Technol. Lett.*, *4*, 2–6, 1991.

Waters, J., Microwave limb sounding, in *Atmospheric Remote Sensing by Microwave Radiometry*, edited by M. Janssen, chap. 8, John Wiley, New York, in press, 1992.

Waters, J., J. Gustincic, R. Kakar, H. Roscoe, P. Swanson, T. G. Phillips, T. DeGraauw, A. Kerr, and R. Mattauch, Aircraft search for millimeter wavelength emission by stratospheric ClO, *J. Geophys. Res.*, *84*, 6934–7049, 1979.

Waters, J., J. Gustincic, P. Swanson, and A. Kerr, Measurements of upper atmospheric H_2O emission at 183 GHz, in *Atmospheric Water Vapor*, edited by Wilkerson and Ruhnke, pp. 229–240, Academic, San Diego, Calif., 1980.

Waters, J., J. Hardy, R. Jarnot, and H. Pickett, Chlorine monoxide radical, ozone, and hydrogen peroxide: Stratospheric measurements by microwave limb sounding, *Science*, *214*, 61–64, 1981.

Waters, J., J. Hardy, R. Jarnot, H. Pickett, and P. Zimmermann, A balloon-borne microwave limb sounder for stratospheric measurements, *J. Quant. Spectrosc. Radiat. Transfer*, *32*, 407–433, 1984.

Waters, J., R. Stachnik, J. Hardy, and R. Jarnot, ClO and O_3 stratospheric profiles: Balloon microwave measurements, *Geophys. Res. Lett.*, *15*, 780–783, 1988.

F. T. Barath, M. C. Chavez, R. E. Cofield, D. A. Flower, M. A. Frerking, M. B. Gram, W. M. Harris, J. R. Holden, R. F. Jarnot, W. G. Kloezeman, G. J. Klose, G. K. Lau, M. S. Loo, R. P. McKinney, H. M. Pickett, G. Siebes, F. S. Soltis, J. A. Tarsala, J. W. Waters, and W. J. Wilson, Jet Propulsion Laboratory, California Institute of Technology, Pasadena, CA 91109-8099.

B. J. Maddison, Rutherford Appleton Laboratory, Oxfordshire, England.

R. J. Mattauch, University of Virginia, Charlottesville, VA 22903.

G. E. Peckham and R. A. Suttie, Heriot-Watt University, Edinburgh, Scotland.

(Received June 23, 1992;
revised January 25, 1993;
accepted January 25, 1993.)